THE ARCHIVES OF TRANSPORT
VOL. XXVII-XXVIII NO 3-4 2013

Powertrain system with an ultracapacitor-based auxiliary energy storage for an urban battery electric vehicle

Piotr Biernat*
Piotr Rumniak*
Marek Michalczuk*
Andrzej Gałecki*
Lech Grzesiak*
Bartłomiej Ufnalski*
Arkadiusz Kaszewski*

Received October 2013

Abstract

This paper presents a powertrain system for an urban electric vehicle. The powertrain system consists of a hybrid energy source (battery storage and ultracapacitors) and drivetrain system (two in-wheel outer-rotor PMSMs). Battery performance improvement has been achieved by supporting it with ultracapacitor energy storage. Power flow control using fuzzy logic controller is presented in detail. An electronic differential algorithms have been implemented and tested.

1. Introduction

Current energy-efficient cars can be divided into two main groups: hybrid electric vehicles (HEV) and battery electric vehicles (BEV). HEV combines a conventional internal combustion engine (ICE) with an electric motor. BEV is a pure electric vehicle with battery energy storage and electric propulsion system. Due to possibility of using

* Warsaw University of Technology, Faculty of Electrical Engineering, Institute of Control and Industrial Electronics, Poland

direct drive system, BEVs allow for a significant reduction of moving or rotating elements when compared to ICE systems, and thus improving its reliability [17, 21]. Electric drive (electric motors fed by converters) compared to ICE can reach their maximum torque from zero to nominal speed, which gives the possibility of eliminating the clutch and gearbox. Another key advantage is that electric drives can recover energy during regenerative braking and charge the vehicle's batteries. Unfortunately, due to the low-volume production, high prices and limited battery life span, these types of vehicles are less popular than ICE vehicles.

Nowadays, particularly in the large cities, electric cars are mostly used by public transport (buses) [22] and in commercial transport (electric taxis) [9]. In order to allow a disabled people who use a wheelchair to access the vehicle and be a driver some conditions must be met. This conditions have been provided in the designed electric vehicle (ECO-Car), shown in Fig.1.1. Interior of the ECO-Car allows easy access to the car from three different sides and the steering wheel can be operated directly from the wheelchair. To obtain the flat floor, which does not force disabled person to switch from their wheelchair to car seats, battery energy storage has been placed between the plates of the floor and PMSMs (Permanent Magnet Synchronous Motor) have been placed inside the rear wheels.

The topology of the converters and their construction are given in Section II. In Section III control of hybrid energy source is introduced. Section IV describes motor control structure with electronic differential. Conclusions that have been drawn from the present work are summarized in Section V.

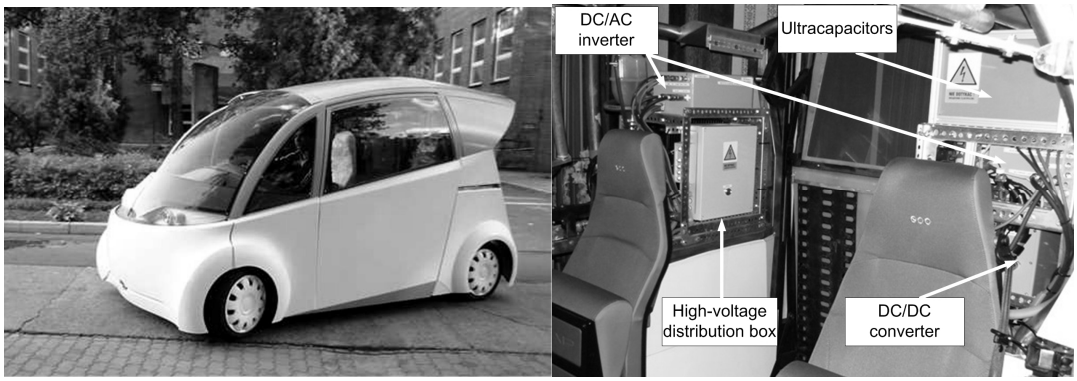

Fig. 1.1. Electric vehicle and selected components of its powertrain system

2. Power electronic converters

Power electronic system consists of two main parts – two drive inverters and two DC/DC converters (Fig. 2.1.). The electric vehicle designed is propelled by two PMSMs placed inside the rear wheels. Speed and torque control of each motor is provided by the individual three-level three-phase neutral point clamped inverters controlled by TMS320F28335 microcontrollers. Drivetrain system is fed by a hybrid energy source

(electrochemical batteries supported by ultracapacitors). There are many possible topologies for a battery and ultracapacitor hybrid [10, 13]. For the described vehicle (ECO-Car) full active hybrid system is used. In this solution electrochemical batteries and ultracapacitors are connected to DC-link circuit through individual interleaved bidirectional converters.

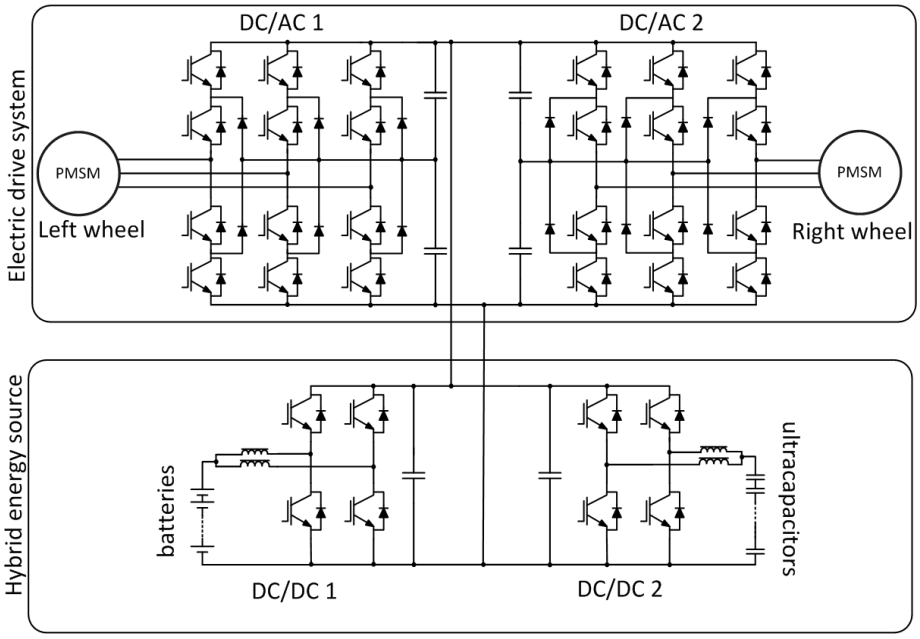

Fig. 2.1. Electrical diagram of the ECO-Car powertrain architecture

2.1 DC/AC inverters for the drivetrain system

The most popular converter topology for three-phase motor is two-level voltage source inverter (VSI) presented in Fig. 2.2a. Generated square wave output voltage causes motor current ripples, the effects of which are electromagnetic torque ripples.

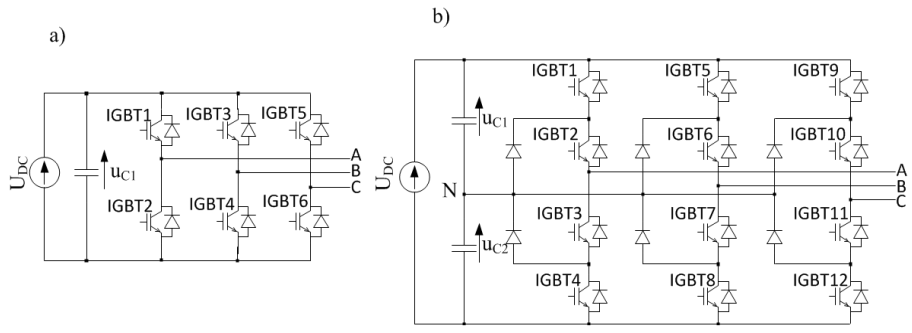

Fig. 2.2. Topology of the converters: a) two-level, b) three-level

To improve inverter output voltage and reduce current ripples, the three-level neutral point clamped inverter (Fig. 2.2b) is used [12]. The output signal spectrum is significantly improved in comparison to classic two-level converters [12]. Comparing phase to phase output voltage (Fig. 2.3), where the switching frequency (5 kHz), fundamental harmonic of the output voltage and DC-link voltage were equal, it can be noticed that three-level converter output voltage (Fig. 2.3b) is more similar to sinusoidal wave than for two-level converter (Fig. 2.3a).

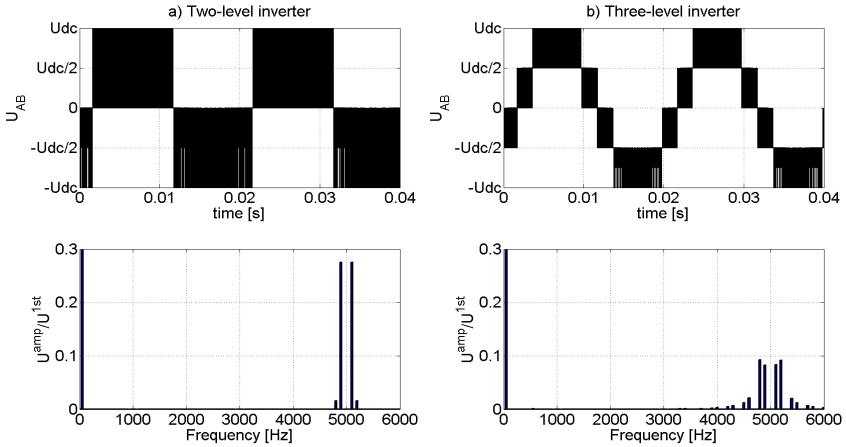

Fig. 2.3. Phase to phase output voltages and their signal spectrum: a) two-level converter, b) three-level converter

VSIs designed for the ECO-Car are comprised of: interface board with microcontroller, measurement sensors, transistor modules, transistor drivers, DC-link capacitors, liquid-cooled heatsink, housing with input and output connectors. In the table 2.1 selected physical and electrical inverter parameters are shown.

Table 2.1

Physical parameters of the DC/AC inverters

Dimensions	321 x 211x 150 mm
Weight	7,5 kg
Volume	10 dm^3
Specific Power	5,1 kW/kg
Power Density	3,8 kW/dm^3
Max. input DC voltage	650 V_{dc}
Output phase-to-phase voltage	350 V_{rms}
Output phase current	42A_{rms}

The first layer of the VSI structure consists of a base to which heatsink and DC-link capacitors are connected. DC-link capacitors in a rectangular case together with the liquid-cooled aluminium heatsink allow for the efficient use of space for combining with the rest

of the components. The PCB with high voltage circuit (DC-bus) is soldered to three modules fixed to the heatsink. Two current sensors are used to measure motor currents.

Fig. 2.4. Voltage source inverter for ECO-Car: a) DC voltage measurement board, b) control board with microcontroller and FPGA unit, c) low voltage power supply board, d) mounting plate, e) IGBTs driver boards, f) DC-link board, g) IGBT modules, h) heatsink

The VSI housing construction protects the device from external factors, e.g. water and dust. Front panel of the device contains connectors such as: low voltage supply (24V supply), encoder (ENC), can bus (CAN), DC-link voltage (IN), output voltage (OUT) and cooling.

2.2 DC/DC converter design

The hybrid energy source is the combination of electrochemical batteries and the additional ultracapacitor energy storage which supports the main source in the dynamic states. To control power flow between electrochemical batteries, ultracapacitors and drivetrain two DC/DC converters are used. DC/DC converters are also designed as layered structure (Fig. 2.5) enclosed in one sealed housing. These devices are composed of: voltage and current sensors, temperature sensors, liquid-cooled heatsink, transistor modules and interface board with the microcontroller. Physical and electrical parameters of the designed device are shown in the table 2.2.

Table 2.2

Physical parameters of the DC/DC converter

Dimensions	292 x 210 x 208 mm
Weight	8,5 kg
Volume	12,75 dm^3
Specific Power	6,35 kW/kg
Power Density	4,23 kW/dm^3
Battery voltage	295 V
Max. Battery current (continuous)	20 A
Ultracapacitors voltage	485 V
Max. Ultracapacitors current (continuous)	20 A
Max. output DC voltage	650 V

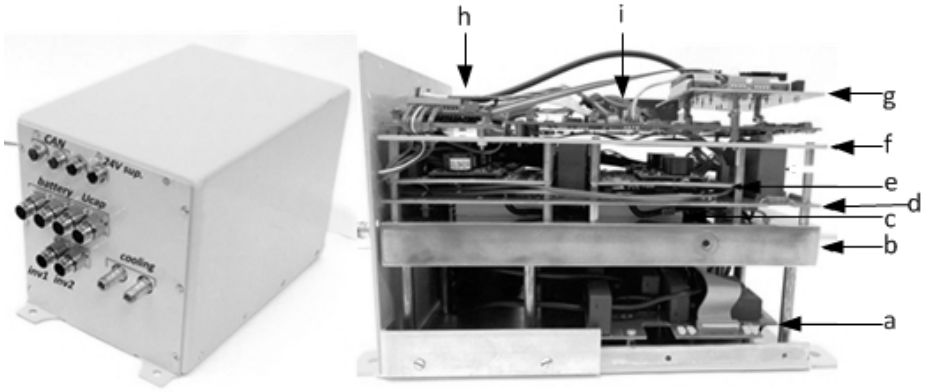

Fig. 2.5. DC/DC converter: a) voltage and current measurements board, b) heatsink, c) IGBT modules, d) DC-link board, e) IGBTs driver boards, f) mounting plate, g) low voltage power supply board, h) temperature measurement board, i) control board with microcontroller and FPGA unit

2.3 Universal control interface

All control algorithms are implemented in the digital TMS320F28335 signal processor located on the interface board. The interface board shown in Fig. 2-6 contains:
- microcontroller TMS320F28335 (manufacturer: Texas Instruments),
- FPGA CYCLONE II EP2C8 (manufacturer: Altera),
- 32 PWM (pulse width modulation) outputs,
- 16 ADC (analogue-to-digital converter) channels,
- 64kb EEPROM memory,
- alphanumeric LCD display support,
- SPI interface,
- JTAG emulator XDS 100 v2,

- USB 2.0,
- CANbus (two independent buses),
- RS232 serial communication
- 10 digital input/output ports
- 16 inputs for error signal from drivers
- 16 isolated digital inputs (differential signals)
- 8 isolated digital outputs (differential signals)

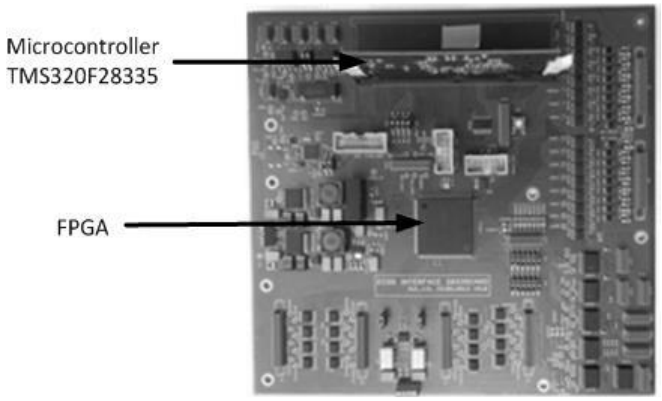

Fig. 2.6. The interface board with TMS320F28335 microcontroller and FPGA

Each converter is controlled by individual microcontroller through the interface board connectors (Fig. 2.6.).

The signals used to control each VSI are: 12 PWM outputs, 4 analogue inputs for voltage and current measurements, 5 analogue inputs for temperature measurements, digital input/output for encoder and 3 connectors for CANbus communication. In case of the signals used to control the DC/DC converter it can be distinguished: 8 PWM outputs, 7 analogue inputs for voltage and current measurements, 4 analogue inputs for temperature measurement and 3 connectors for CANbus communication.

3. Hybrid energy source

Electrochemical batteries are the most common energy storage for electric vehicles. Leading position in on-board energy sources is occupied by lithium-ion battery. However none of batteries available on the market fully meets the expectations of performance in the context of electric vehicle. Due to the nature of chemical reactions, power density decreases significantly with falling temperature. A lack of sufficient power needed for maintaining desired vehicle dynamics manifests itself especially if the battery pack has low capacity [15, 16]. Moreover, high battery temperature and current also reduce the battery life [20]. Battery performance improvement can be achieved by using additional ultracapacitors, which will reduce the battery current in dynamic states [1, 2]. The main advantages of this hybridization are: extended lifetime of the main storage, increased

efficiency of energy recovery and the ability to provide required power over wide temperature range.

The main energy storage for ECO-Car consists of 92 LiFePO4 cells with capacity of 40Ah. Such energy storage, provides ca. 80 km driving range at 80% depth of discharge in nominal conditions. Battery pack is placed between the plates of the floor (Fig. 3.1.). An auxiliary energy storage consists of 176 ultracapacitor cells with a capacity of 310F. Key parameters of the hybrid energy storage are presented in table 3-1.

Fig. 3.1. Electrochemical battery pack placed in the chassis (left) and ultracapacitor energy storage (right)

Table 3.1

Properties of energy storages

Parameter	$LiFePO_4$ pack	Ultracapacitor stack
Nominal voltage	295 V	485 V
Capacity of cell	40 Ah	310 F
Number of cells	92	176
Stored energy	12 kWh	55 Wh
Mass of cells	140 kg	11 kg
Rated Power	6 kW	8 kW
Max Power	35 kW	70 kW

In view of the high currents at low voltage of ultracapacitors, voltage operating range has been limited from below by half of the nominal voltage. In this case, usable energy is 75% of the total stored energy. Due to space and cost concerns ultracapacitor energy storage has been reduced to a size that allows capturing 40 Wh energy during regenerative braking. This energy reserve enables energy recovery during braking for a vehicle of 1400kg weight, moving at the maximum planned speed of 60 km/h, taking into account the work of resistance force for the deceleration at 5km/h/s and assuming 85% efficiency of the drive system.

The fully active hybrid system (Fig. 2.1), which uses two power converters cooperating with each storage, allows to control the output voltage regardless of both storages' state of

charge. The main purposes of the power management algorithm for hybrid storage are both power division between storages as well as control of ultracapacitors voltage level. The battery should cover average power demand and an auxiliary energy storage should be engaged during high power loads and regenerative braking. Maintaining an adequate ultracapacitors state of charge is particularly important due to the fact that useful energy stored in ultracapacitors (40 Wh with discharge up to half of the nominal voltage) is less than the kinetic energy of the vehicle at maximum speed (55 Wh). This means that the power during acceleration cannot be provided solely from the auxiliary storage.

A schematic representation of the control topology is shown in Fig. 3.2. There are two inner current control loops associated with two DC/DC converters. Maintaining desirable output voltage of the hybrid source along with voltage of UCs as well as appropriate power partitioning between two energy sources is achieved by an adequate reference current value determination by means of fuzzy logic controller.

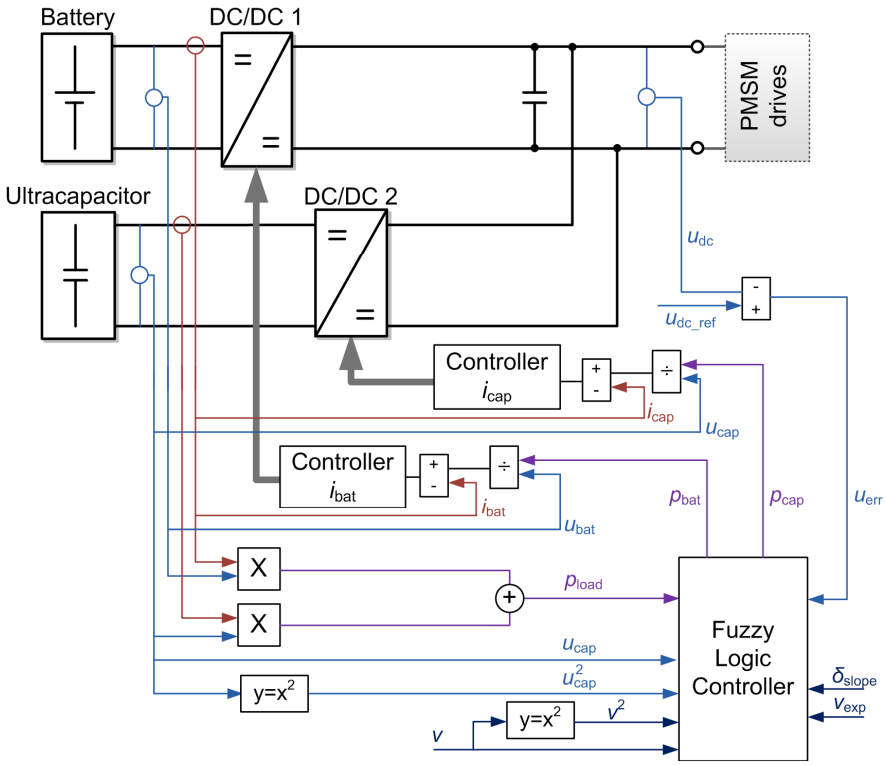

Fig. 3.2. Control diagram for the hybrid energy storage.

The fuzzy logic controller has eight inputs and two output variables. The input variables are: output voltage error of the hybrid source (u_{err}), power load (p_{load}), speed (v), and ultracapacitors voltage (u_{cap}), square of speed normalized to the maximum value (v^2), square of ultracapacitors voltage normalized to the maximum value (u_{cap}^2). Optionally, information on the terrain slope (δ_{slope}) and expected speed of the vehicle (v_{exp}) is also used.

A new trend in the automotive industry is the development of communication technologies for the exchange of information between vehicles on the road (V2V) and between vehicles and the road infrastructure (I2V/V2I) [4,18]. These systems are especially dedicated to improving road safety and traffic management. Information flow from the road infrastructure or vehicles moving in front of us can also help improve the efficiency of power management systems in a hybrid power source for electric vehicle. Vehicle communication systems offer the potential of providing information on the expected speed. This information can be used to better adjust ultracapacitors state of charge and efficient battery power impulses reduction. An instantaneous load power is strongly affected by a terrain. Driving uphill requires maintaining a larger energy reserve due to higher power impulses during accelerating and a lower energy recovery. The opposite case concerns driving downhill, when power consumption is lower and the energy recovery increases. Information about slope of the terrain can be provided by a GPS navigation system.

The output variables of fuzzy logic controller are: battery power (p_{bat}) and ultracapacitors power (p_{cap}). Battery power and ultracapacitor power as a function of selected input variables are shown in Figs. 3.3, 3.4.

The values of v^2 and $u_{cap}{}^2$ are normalized to v_{max}^2 (v_{max} = 60 km/h) and u_{max}^2 (u_{max} = 485V). Variables u_{err}, p_{load}, v, u_{cap}, v_{exp} determine the energy flow between storages and the drive system. Exemplary rules that use this variables are as follows:

1) if (p_{load} is large) and (u_{cap} is not under) and (v_{exp} is high) then (p_{bat} is zero) and (p_{cap} is neg_large);
2) if (p_{load} is mid) and (v is mid) and (u_{cap} is not under) and (v_{exp} is high) then (p_{bat} is zero) and (p_{cap} is neg_small);
3) if (p_{load} is small) and (v is low) and (u_{cap} is not under) and (v_{exp} is high) then (p_{bat} is zero) and (p_{cap} is neg_small);
4) if ($\underline{u}_{err}$ is neg_large) and (u_{cap} is not over) then (p_{bat} is zero) and (p_{cap} is pos_large);
5) if (u_{err} is neg_large) and (u_{cap} is over) then (p_{bat} is pos_large) and (p_{cap} is zero).

On the basis of variables , v^2 and δ_{slope} the power component responsible for the energy exchange between storages is calculated. Examples of these fuzzy rules are as follows:

6) if ($u_{cap}{}^2$ is low) and (v^2 is high) then (p_{bat} is pos_large) and (p_{cap} is neg_large);
7) if ($u_{cap}{}^2$ is high) and (v^2 is low) and (δ_{slope} is not uphill) then (p_{bat} is pos_large) and (p_{cap} is neg_large);
8) if ($u_{cap}{}^2$ is high) and (v^2 is zero) and (δ_{slope} is downhill) then (p_{bat} is pos_large) and (p_{cap} is neg_large).

Power component responsible for the energy exchange is equal for the two sources, but with the opposite sign. Positive values of the power mean that energy storage is being charged.

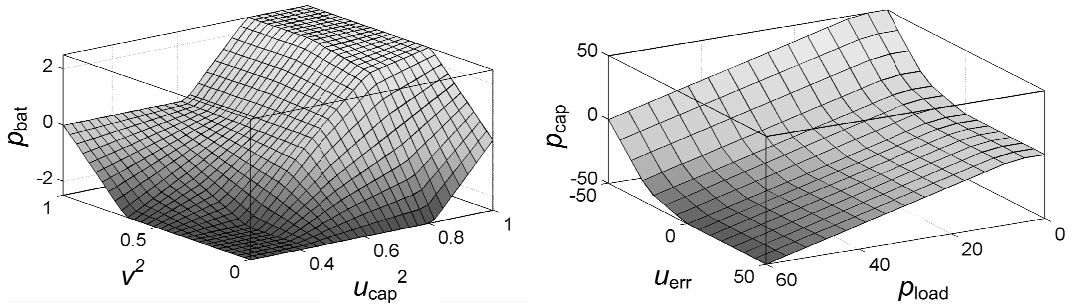

Fig. 3.3. Relationships between u_{cap}^2, v^2 and p_{cap}, when δ_{slope} is flat (left) and ultracapacitor power (p_{cap}) as a function of the output voltage error (u_{err}) and load power (p_{load}), when v=30km/h, u_{cap}=350V i v_{exp}=60km/h (right)

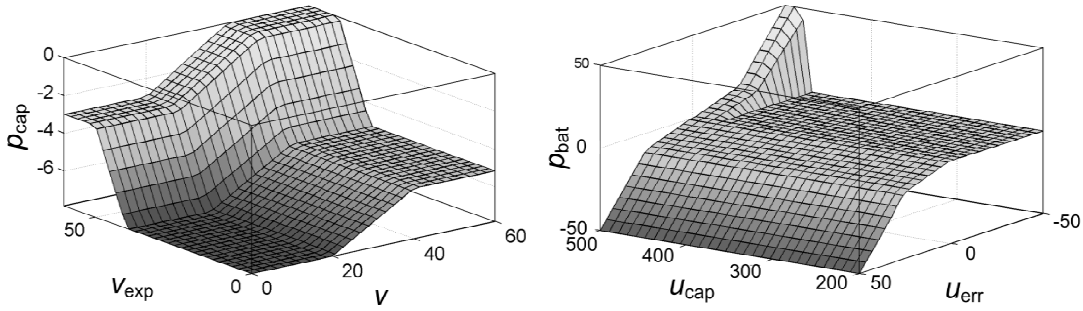

Fig. 3.4. Relationships between v_{exp}, v and p_{cap}, when u_{err}=0V, p_{load}=8kW, u_{cap}=350V (left) and battery power (p_{bat}) as a function of the output voltage error (u_{err}) and voltage ultracapacitor (u_{cap}), when v=30km/h, p_{load}=0 and v_{exp}=60km/h (right)

3.2 Simulation and experimental results

The fuzzy controller developed has been tested during the simulation studies using the active hybrid energy source model described in [20]. The nonlinear control algorithm of the energy flow uses information about the expected slope of the terrain and expected speed. An effect of using information on expected speed of the vehicle is presented for urban driving cycle recorded at rush hours (Fig. 3.5a). The basic operating mode, without the use of information on the expected vehicle speed, does not reduce battery power impulses at their low value (Fig. 3.5b). Availability of information about high traffic and low driving speed results in an almost complete coverage of power demand by the ultracapacitors (Fig. 3.5c).

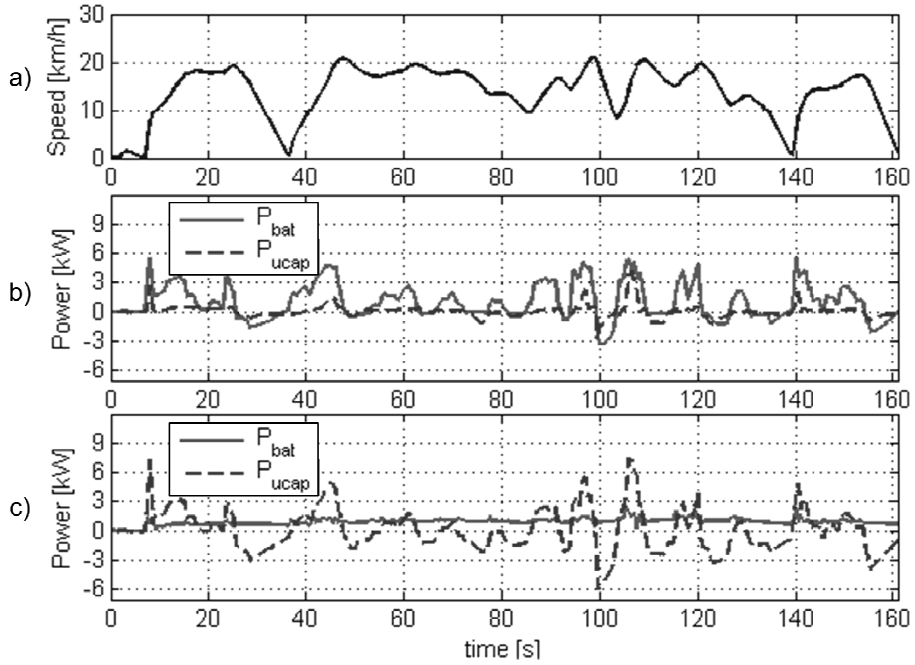

Fig. 3.5. Speed (a) and power distribution without the use of v_{exp} signal (b), and when signal v_{exp} is available (c)

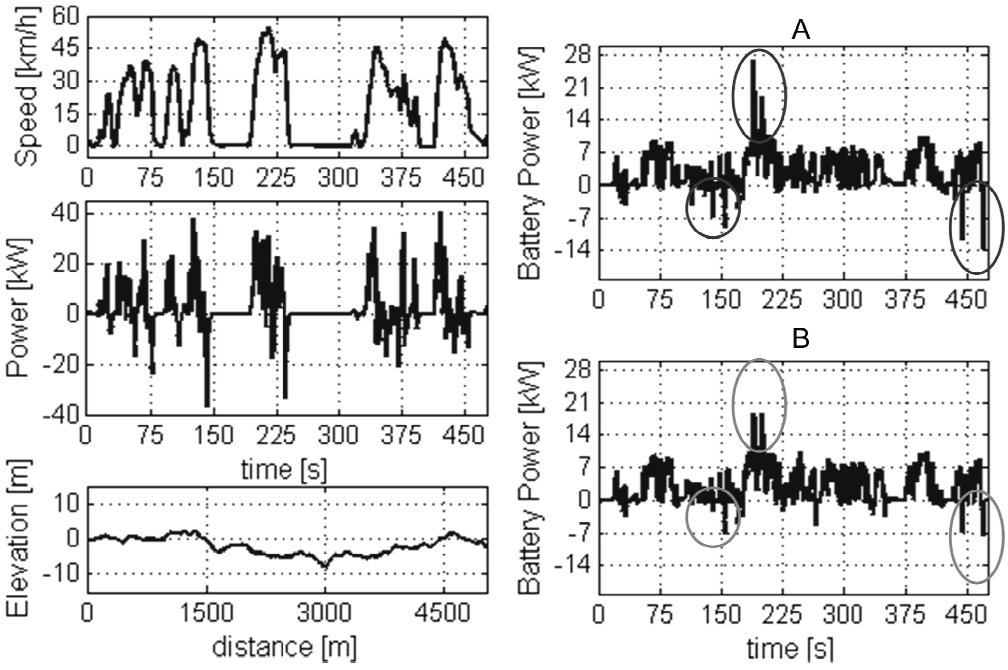

Fig. 3.6. Real driving cycle profiles (left). Battery power in real cycle when the slope information is not used (A) and is used (B)

Figure 3.6 shows the speed profile for the dynamic real driving (recorded using GPS receiver) in the urban area of Pruszków. Power drawn from the battery is compared for two cases: when the information on the slope of terrain is not used (Fig. 3.6a) and when this information is available (Fig. 3-6b). Both positive and negative battery power impulses are being reduced when topography of the route is known. It is particularly distinctive e.g. in 140, 190, and 440 second, as it is indicated in Fig. 3-8. The last example highlights the fact that the additional information from navigation systems can be beneficial and should be included in the algorithm.

Validation of the proposed power management algorithm was performed through experimental tests on non-mobile laboratory setup (Figure 3-7) with two motor sets. In each motor set, one PMSM is operated as a drive, the other PMSM is operated as a load. Load machines emulate resistance forces occurring during drive. The PMSMs are fed by four three-level inverters. Hybrid source in laboratory setup consists of grid supplied active rectifier with DC/DC converter, which substitutes the battery energy storage, and ultracapacitors controlled by DC/DC converter. Depending on the vehicle, non-mobile systems have been designed for reduced power (scale of 1:10).

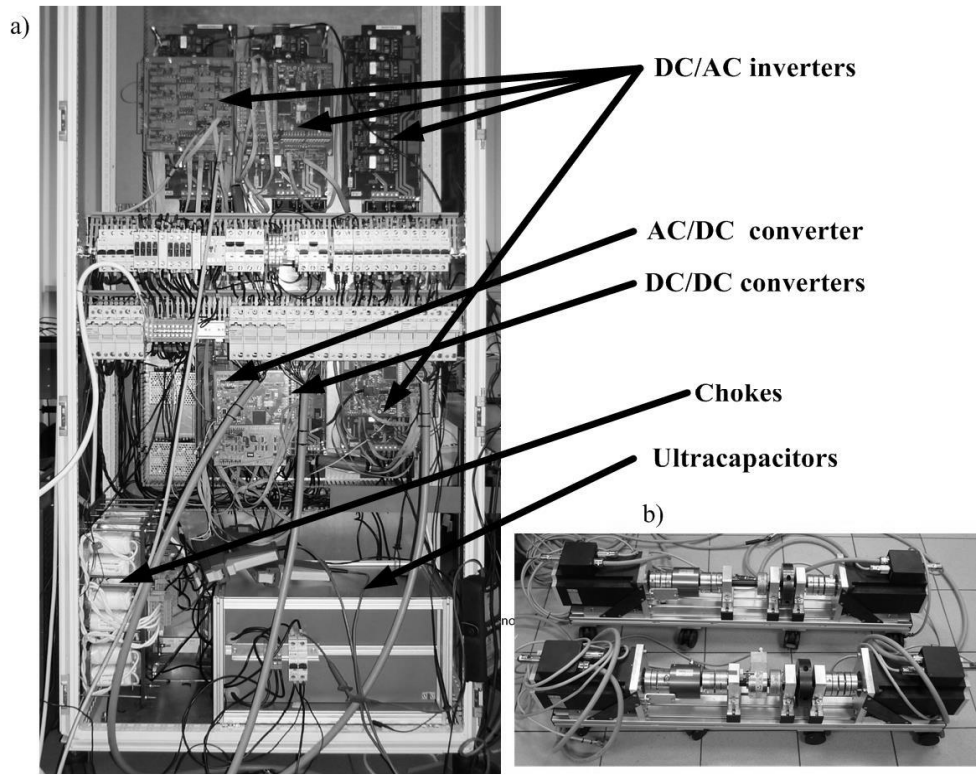

Fig. 3.7. Laboratory setup: a) power electronic equipment, b) four-motor set

Figure 3.8 shows power division between storages for driving cycle with constant acceleration. Peak power of laboratory drive system for the presented speed profile is equal

to 4kW. Supporting main storage by ultracapacitors allows almost four times reduction of main source power without deterioration of vehicle dynamics.

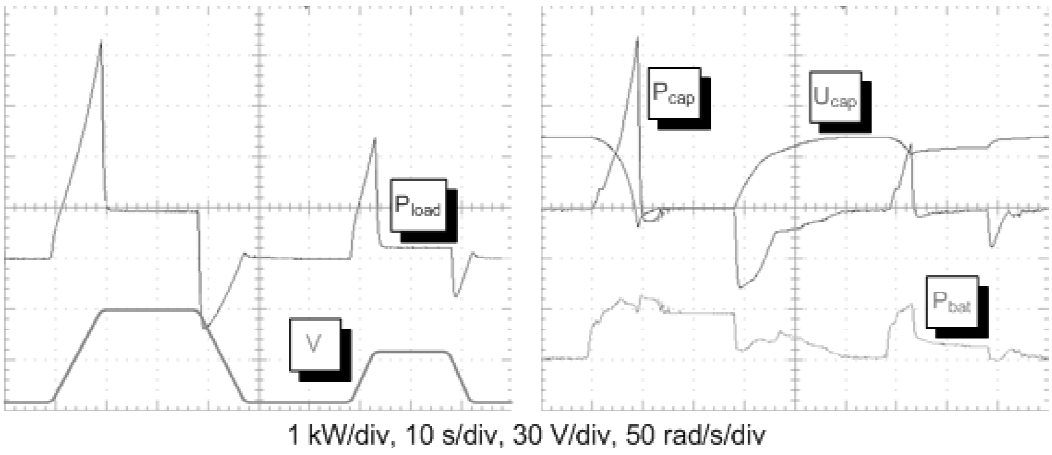

Fig. 3.8. Speed and corresponding power provided by main source and auxiliary ultracapacitor source

Figure 3.9 shows the distribution of power during driving uphill, where there is no possibility of supporting by ultracapacitors at the same extent as in the case of driving on flat roads, due to the increased power consumption of the drive system. This results in main source impulse power at the final stage of acceleration (at ca. 20s). However, despite the lack of energy in the supporting energy storage, the control algorithm does not allow ultracapacitors to be fully discharged before the top speed of the vehicle is reached. Even in the final stage of acceleration the demand for power has been partially covered by ultracapacitors.

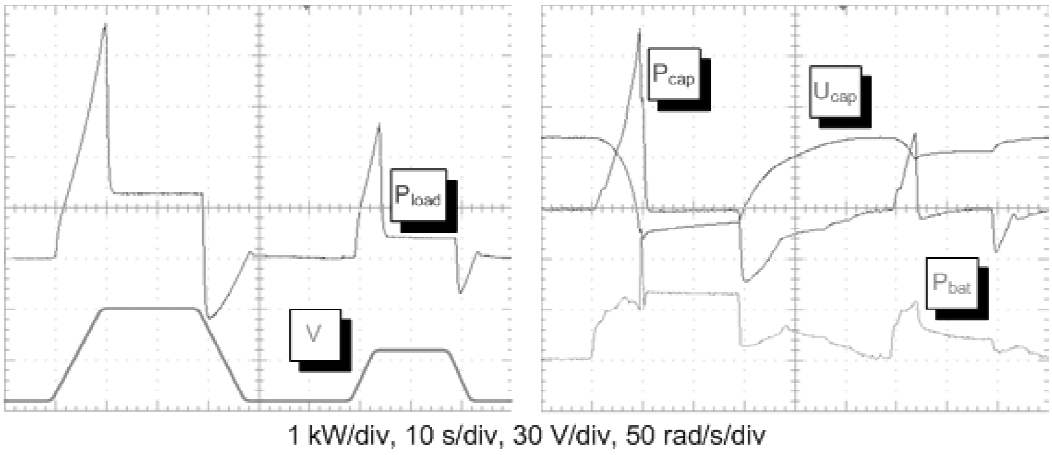

Fig. 3.9. Speed and corresponding power provided by main source and auxiliary ultracapacitor source during driving uphill

4. Electronic differential

The electronic differential allows for different wheel speeds. This feature is needed when the vehicle is cornering. In the drive system propelled by direct drive (two independent rear wheel drives), torques cannot be split up by mechanical differential. Therefore, the electronic differential is needed.

Figure 4.1 depicts the control structure of the electronic differential which allows to operate with speed or torque reference signal. The control structure is implemented as a distributed system. Communication between control units is performed through CAN-bus. Master controller 'M' receives angular speeds of driving wheels from slave controllers 'L' and 'R'. Vehicle linear speed is calculated from angular speeds (assuming no slip). Reference speeds ω_L^{ref}, ω_R^{ref} or torque T^{ref}, depending on which electronic differential is used, are calculated from the information on setting potentiometers attached to rings on the steering wheel [7], steering angle and angular speed of the wheels. The master controller passes these values to the slave controllers.

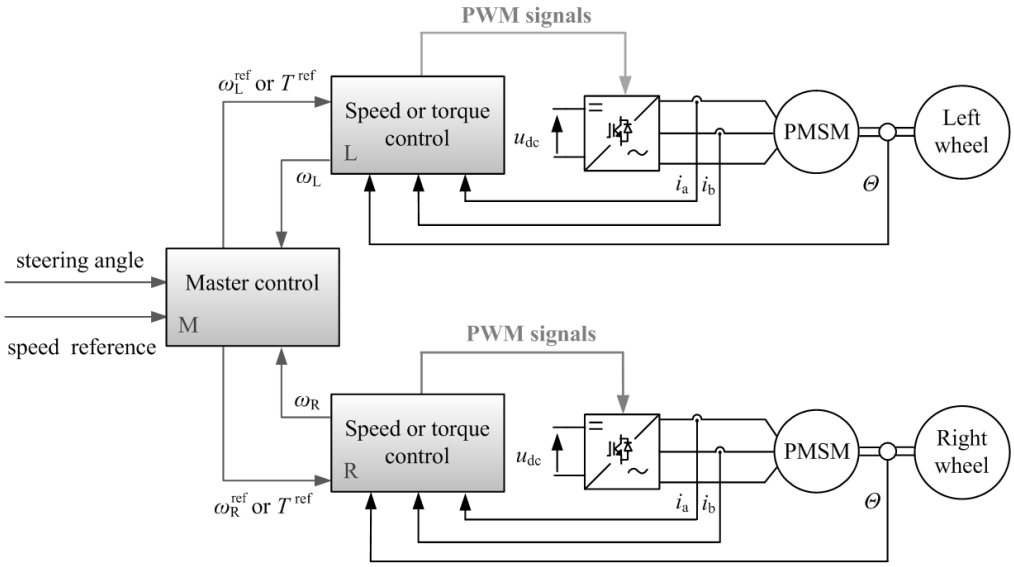

Fig. 4.1. The control structure of the electronic differential.

Two versions of electronic differential and their experimental results are presented in this section. The electronic differential control structure with the average speed controller is shown in Fig. 4.2 [2, 15, 22]. In this structure position of the potentiometer attached to rings on the steering wheel represents the reference value of motors' average speed, which is proportional to the vehicle linear speed (assuming no slip). The vehicle speed v is given by:

$$v = 0.5 \cdot (\omega_L + \omega_P) \cdot R_d \tag{1}$$

where:
v - vehicle linear speed [m/s],

ω_L - angular speed of the left wheel [rad/s],
ω_R - angular speed of the right wheel [rad/s],
R_d - tire radius [m].

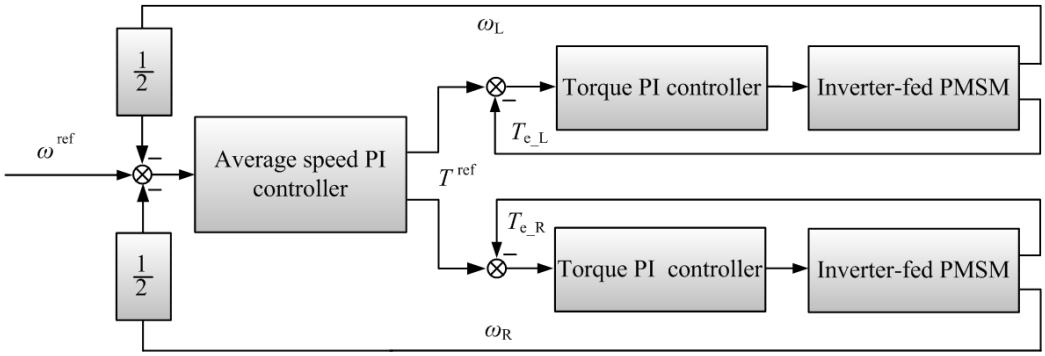

Fig. 4.2. The electronic differential topology with the average speed controller

In this solution reference torque values for the two drive wheels are equal regardless of their speed difference. A disadvantage of this structure is the loss of the torque transmission, when one wheel slips.

Figure 4.3 depicts waveforms of the reference speed, angular speeds and electromagnetic torques obtained from vehicle turning right (7s < t < 13s). During the turning manoeuvre the difference between wheels angular speed can be observed and torques remain the same.

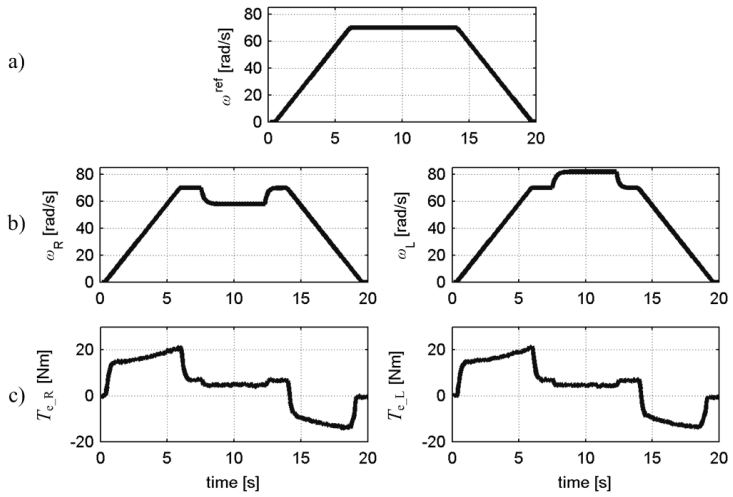

Fig. 4.3. The results of the experiment with the average speed controller: a) reference speed ω^{ref}, b) measured speeds ω_L, ω_R, c) electromagnetic torques T_{e_L}, T_{e_R}

The second topology of the electronic differential contains an Ackermann steering model [6, 8, 14]. This structure is presented in Fig. 4.4. In view of the separate speed controllers for left and right wheel, the difference in speeds during turnings has to be calculated explicitly. One of the models that calculates reference angular speeds is the Ackermann steering model which is described by the following equations [19]:

$$\omega_{\mathrm{L}}^{\mathrm{ref}} = \frac{v}{R_{\mathrm{d}}} \cdot \left(1 + \frac{D}{2L} \cdot \mathrm{tg}(\delta)\right) \tag{2}$$

$$\omega_{\mathrm{R}}^{\mathrm{ref}} = \frac{v}{R_{\mathrm{d}}} \cdot \left(1 - \frac{D}{2L} \cdot \mathrm{tg}(\delta)\right) \tag{3}$$

$$\Delta\omega = 0.5 \cdot \left(\omega_{\mathrm{L}}^{\mathrm{ref}} - \omega_{\mathrm{R}}^{\mathrm{ref}}\right) \tag{4}$$

where:
$\omega_{\mathrm{L}}^{\mathrm{ref}}$ - left rear wheel reference angular speed [rad/s],
$\omega_{\mathrm{R}}^{\mathrm{ref}}$ - right rear wheel reference angular speed [rad/s],
L - wheelbase [m],
δ - steering angle [rad],
D - tread [m].

This structure requires precise steering geometry information, but does not lose torque transmission for both wheels if one wheel slips.

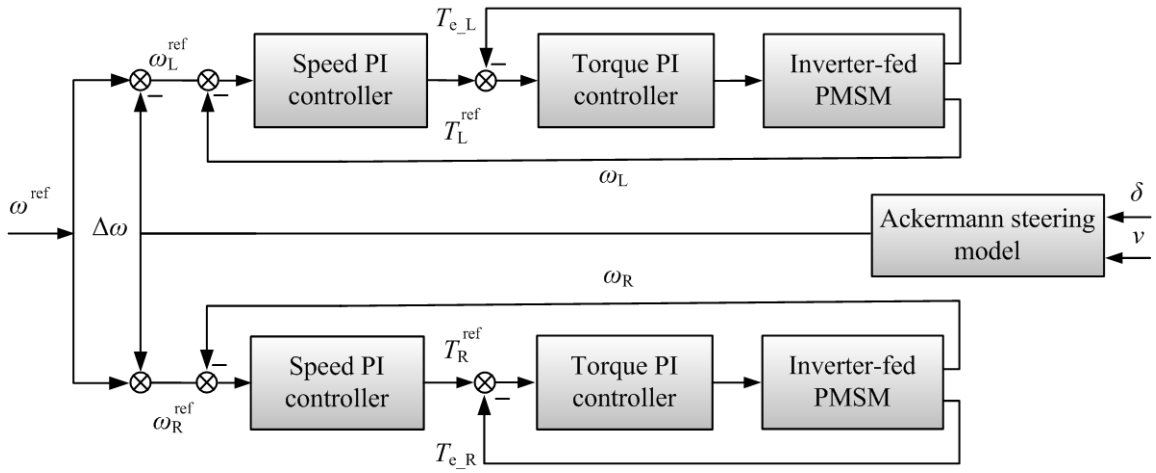

Fig. 4.4. Topology of the electronic differential with the Ackermann steering model

Waveforms of reference speeds, angular speeds and electromagnetic torques are shown in Fig. 4.5. In this test the vehicle is turning right ($7\mathrm{s} < \mathrm{t} < 9\mathrm{s}$) and then turning left ($11\mathrm{s} < \mathrm{t} < 13\mathrm{s}$) with constant speed. It can be noticed that torques waveform are different in the dynamic states because outputs of speed controllers are not equal $T_{\mathrm{L}}^{\mathrm{ref}} \neq T_{\mathrm{R}}^{\mathrm{ref}}$.

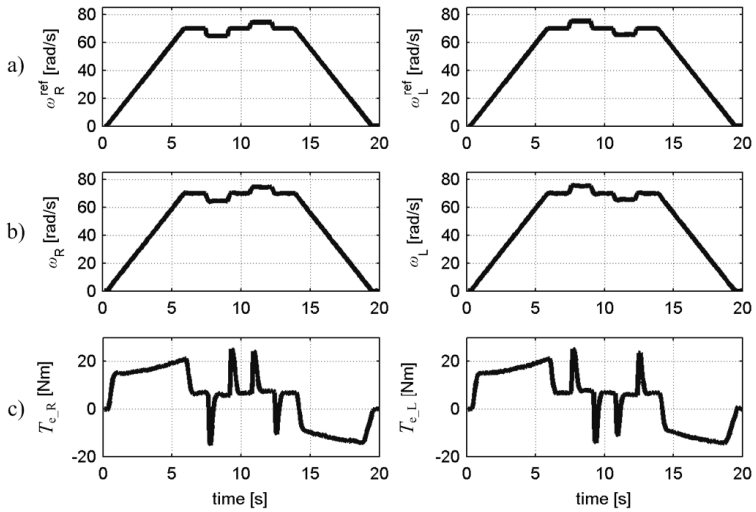

Fig. 4.5. A results of the experiment with the Ackermann steering model: a) reference speeds ω_L^{ref}, ω_P^{ref}, b) measured speeds ω_L, ω_R, c) electromagnetic torques T_{e_L}, T_{e_R}

5. Conclusions

The powertrain system designed for the electric vehicle has been presented. The hybrid energy storage allows for efficient use of energy. Simulation and experimental results confirmed that combination of lithium batteries and ultracapacitors improves performance and reliability of the storage. To reduce power impulses drawn from battery, fuzzy logic control takes into consideration additional information, like a slope of a terrain and an expected speed. Two types of wheels speed controls have been presented: the Ackermann steering model and average speed controller. Drive control algorithms with electronic differential, implemented as a distributed control system, have been successfully verified on laboratory setup as well as on the mobile mock-up of the vehicle. The interface boards for microcontroller TMS320F28335 and FPGA have been designed to control converters.

The results obtained for the ECO-Car mock-up confirmed correct operation of all subsystems of the designed powertrain with the hybrid energy storage. An extensive experimental tests are planned to be continued on vehicle mobile mock-up.

Acknowledgement

This article was financed from ECO-Mobility project WND-POIG.01.03.01-14-154/09. The project co-financed from the European Regional Development Fund within the framework of Operational Programme Innovative Economy.

6. References

1. Burke A., Batteries and Ultracapacitors for Electric, Hybrid, and Fuel Cell Vehicles, Proceedings of the IEEE , Volume 95, Issue 4, April 2007, p. 806 - 820.
2. Burke A., Ultracapacitor Technologies and Application in Hybrid and Electric Vehicles, International Journal of Energy Research, Volume 34, Issue 2, February 2010, p. 133-15.
3. de Castro, R.P., Oliveira, H.S., Soares, J.R., Cerqueira, N.M., Araujo, R.E.: A new FPGA based control system for electrical propulsion with electronic differential, Power Electronics and Applications, 2007 European Conference on , vol., no.,pp.1-10, 2007
4. Farah H., Koutsopoulos H. N., Saifuzzaman M., Kölbl R., Fuchs S., Bankosegger D., Evaluation of the effect of cooperative infrastructure-to-vehicle systems on driver behaviour, Transportation research part C: emerging technologies, Volume 21, Issue 1, p. 42-56.
5. Film capacitors - Power electronic capacitors. PCC series for Mild HEV HybridPACK™1. 2009, (www.epcos.com)
6. Gair, S., Cruden, A., McDonald, J., Hredzak B.: Electronic differential with sliding mode controller for a direct wheel drive electric vehicle. Mechatronics, 2004. ICM '04. Proceedings of the IEEE International Conference on , s. 98- 103, 2004
7. Grabarek I., Choromański W.: Innovative environment at design in means and systems of transport with particular emphasis on the human factor., Advances in Human Aspects of Road and Rail Transportation, edited by Neville A. Stanton, CRS Press Taylor&Francis Group, 2012, ISBN 978-1-4398-7123-2, pp.273-282,
8. Grzesiak L. M., Ufnalski B., Kaszewski A., Michalczuk M., Rumniak. P., Gałecki A., Biernat P.: Power Electronic Drive System for an Urban Electric Vehicle with a Hybrid Energy Storage - The Physical Emulator and the Mobile Mockup. Zeszyty Problemowe - Maszyny Elektryczne nr. 98, wyd. BOBRME Komel, s. 79-88, 2013
9. http://www.greencapitalcity.pl/ecocar-system.html, (in polish).
10. Kohler T. P., Buecherl D., Herzog H.-G., Investigation of control strategies for hybrid energy storage systems in hybrid electric vehicles, IEEE Vehicle Power and Propulsion Conference, 2009, p.1687-169.
11. Kozłowski M., Choromanski W.: Dynamics simulation studies on the electric city car with an electromechanical differential and the rear wheels drive. Bulletin of the Polish Academy of Sciences: Technical Sciences, Volume 61, No. 3, 2013
12. Krug D., Bernet S., Fazel S. S., Jalili K. and Malinowski M.: Comparison of 2.3-kV Medium-Voltage Multilevel Converters for Industrial Medium-Voltage Drives, IEEE Transaction on industrial Electronics, Vol. 54, No. 6, December 2007, pp.2979-2992
13. Kuperman A., Aharon I., Battery-ultracapacitor hybrids for pulsed current loads: A review, Renewable and Sustainable Energy Reviews Volume 15, Issue 2, February 2011, p. 981-992.
14. Magallan, G.A., De Angelo, C.H., Bisheimer, G., Garcia, G.: A neighborhood electric vehicle with electronic differential traction control, Industrial Electronics, IECON 2008. 34th Annual Conference of IEEE , vol., no., pp.2757-2763, 2008
15. Michalczuk M., Grzesiak L.M., Ufnalski B., "A lithium battery and ultracapacitor hybrid energy source for an urban electric vehicle", Electrical Review, vol. 04b, 2012, p. 158-162
16. Michalczuk M., Grzesiak L.M., Ufnalski B., Hybridization of the lithium energy storage for an urban electric vehicle, Bulletin of the Polish Academy of Sciences: Technical Sciences, Volume 61, Issue 2, 2013, p. 325-333.
17. Rudnicki T.: Exploitation costs of an electric vehicle. Zeszyty Problemowe - Maszyny Elektryczne nr 97, wyd. BOBRME Komel, s. 49-52, 2012
18. Sukuvaara T., Pomalaza-Ráez C.,Vehicular Networking Pilot System for Vehicle-to-Infrastructure and Vehicle-to-Vehicle Communications, International Journal of Communication Networks and Information Security (IJCNIS), Volume 1, Issue 3, December 2009,
19. Szumanowski A.: Projektowanie dyferencjałów elektromechanicznych elektrycznych pojazdów drogowych. Wydawnictwo Instytutu Technologii Eksploatacji, Warszawa-Radom, 2007

20. Wang Jiayuan; Sun Zechang; Wei Xuezhe, "Performance and characteristic research in LiFePO4 battery for electric vehicle applications," Vehicle Power and Propulsion Conference, 2009. VPPC '09. IEEE , vol., no., pp.1657,1661, 7-10 Sept. 2009
21. Xiao F. , Deng Q.L., Liu J.C.: Design of direct-drive axial flux permanent magnet inwheel machine for electric vehicle. IEEE Electrical International Conference on Machines and Systems , ICEMS, , pp. 1-4 2011
22. Živanović Z., Nikolić Z.: The Application of Electric Drive Technologies in City Buses, Intech open science , s.165-203, 2012